ARTICLES
https://doi.org/10.1038/s41929-021-00721-y

nature catalysis

Check for updates

Combined anodic and cathodic hydrogen production from aldehyde oxidation and hydrogen evolution reaction

Tehua Wang[1,2,5], Li Tao[1,5], Xiaorong Zhu[3,5], Chen Chen[1], Wei Chen[1], Shiqian Du[1], Yangyang Zhou[1], Bo Zhou[1], Dongdong Wang[1], Chao Xie[1], Peng Long[1], Wei Li[1], Yanyong Wang[1], Ru Chen[1], Yuqin Zou[1]✉, Xian-Zhu Fu[2]✉, Yafei Li[3]✉, Xiangfeng Duan[4]✉ and Shuangyin Wang[1]✉

Hydrogen production through water electrolysis is of considerable interest for converting the intermittent electricity generated by renewable energy sources into storable chemical energy, but the typical water electrolysis process requires a high working voltage (>1.23 V) and produces oxygen at the anode in addition to hydrogen at the cathode. Here we report a hydrogen production system that combines anodic and cathodic H_2 production from low-potential aldehyde oxidation and the hydrogen evolution reaction, respectively, at a low voltage of ~0.1 V. Unlike conventional aldehyde electrooxidation, in which the hydrogen atom of the aldehyde group is oxidized into H_2O at high potentials, the low-potential aldehyde oxidation enables the hydrogen atom to recombine into H_2 gas. The assembled electrolyser requires an electricity input of only ~0.35 kWh per m^3 of H_2, in contrast to the ~5 kWh per m^3 of H_2 required for conventional water electrolysis. This study provides a promising avenue for the safe, efficient and scalable production of high-purity hydrogen.

Hydrogen is a vital feedstock in industrial chemical processes such as ammonia synthesis and is a prospective clean fuel[1–4]. At present, ~95% of the H_2 supply is produced by reforming fossil fuels because of the low cost of this process (US$1.34–2.27 per kg)[5], but this is neither sustainable nor eco-friendly. Despite the promise of water electrolysis as an alternative technology for producing high-purity H_2 (refs. [6–11]), the commercial scalability of this process is limited by its high cost (US$4.15–23.27 per kg)[5], mainly because of the required high-voltage input (for example, 1.6–2.0 V)[12]. Moreover, water electrolysis produces H_2 at the cathode and O_2 at the anode, and the production rates of H_2 and O_2 may in fact be slower than their permeating rates through the membrane at the low power loads that are characteristic of renewable power sources. In extreme cases, gas crossover through the membrane may give rise to explosive H_2/O_2 mixtures[13], posing a considerable safety concern. In addition, the coexistence of H_2/O_2 mixtures and active catalysts may generate reactive oxygen species that damage the membranes in water electrolysers[14]. There is thus keen motivation for developing novel, safe and durable electrolysis systems with low cell voltages and high hydrogen production efficiencies.

Various strategies have been explored to address the above concerns for electrolytic hydrogen production. Researchers have attempted to decouple the water electrolysis reactions using redox mediators, such as $H_6[SiW_{12}O_{40}]$ and $Ni(OH)_2$ (refs. [13,15]). Although the production of H_2 and O_2 is temporally and spatially separated in such systems, high electricity consumption remains an issue because of the large potential gap between the hydrogen evolution reaction (HER) at the cathode and the oxygen evolution reaction (OER) at the anode (>1.23 V, Fig. 1a) and the large overpotentials required to drive these reactions at a practically relevant rate. Another strategy is to replace OER with an organic oxidation reaction that is thermodynamically favourable and economically more attractive[16–21]. Systems employing biomass-derived platform chemicals such as glucose[22,23], furfural[24] and 5-hydroxymethyl furfural (HMF)[25–27] as oxidative reaction substrates are particularly appealing because both the electricity used and the organic feeds are renewable, making the hydrogen production process completely sustainable. Furthermore, the production of value-added organic by-products rather than oxygen can further maximize the return of energy investment. Although the concept of coupling hydrogen production with an organic oxidation reaction has seen much promise and progress, conventional organic electrolyser systems for hydrogen production still require high voltage input (>1 V, Fig. 1a), resulting in high electricity consumption.

Conventional aldehyde (R–CHO) electrooxidation usually proceeds in an alkaline solution catalysed by low-cost transition-metal-based electrocatalysts such as Ni-[28,29], Co-[30,31] and Cu-based[32] materials. In these cases, the aldehyde group is oxidized into the corresponding carboxylate anion, accompanied by the transfer of two electrons, according to

$$R\text{–}CHO + 3OH^- \rightleftharpoons R\text{–}COO^- + 2H_2O + 2e^- \quad (1)$$

Notably, the adsorbed hydrogen atom (*H) originating from the aldehyde group by C–H bond cleavage is easily oxidized into H_2O via the Volmer step ($^*H + OH^- \rightleftharpoons * + H_2O + e^-$) at high potentials of >1.0 V_{RHE}, a potential window for transition-metal-based

[1]State Key Laboratory of Chemo/Bio-Sensing and Chemometrics, College of Chemistry and Chemical Engineering, Advanced Catalytic Engineering Research Center of the Ministry of Education, Hunan University, Changsha, China. [2]College of Materials Science and Engineering, Shenzhen University, Shenzhen, China. [3]Jiangsu Collaborative Innovation Centre of Biomedical Functional Materials, Jiangsu Key Laboratory of New Power Batteries, School of Chemistry and Materials Science, Nanjing Normal University, Nanjing, China. [4]Department of Chemistry and Biochemistry, University of California, Los Angeles, Los Angeles, CA, USA. [5]These authors contributed equally: Tehua Wang, Li Tao, Xiaorong Zhu. ✉e-mail: yuqin_zou@hnu.edu.cn; xz.fu@szu.edu.cn; liyafei@njnu.edu.cn; xduan@chem.ucla.edu; shuangyinwang@hnu.edu.cn

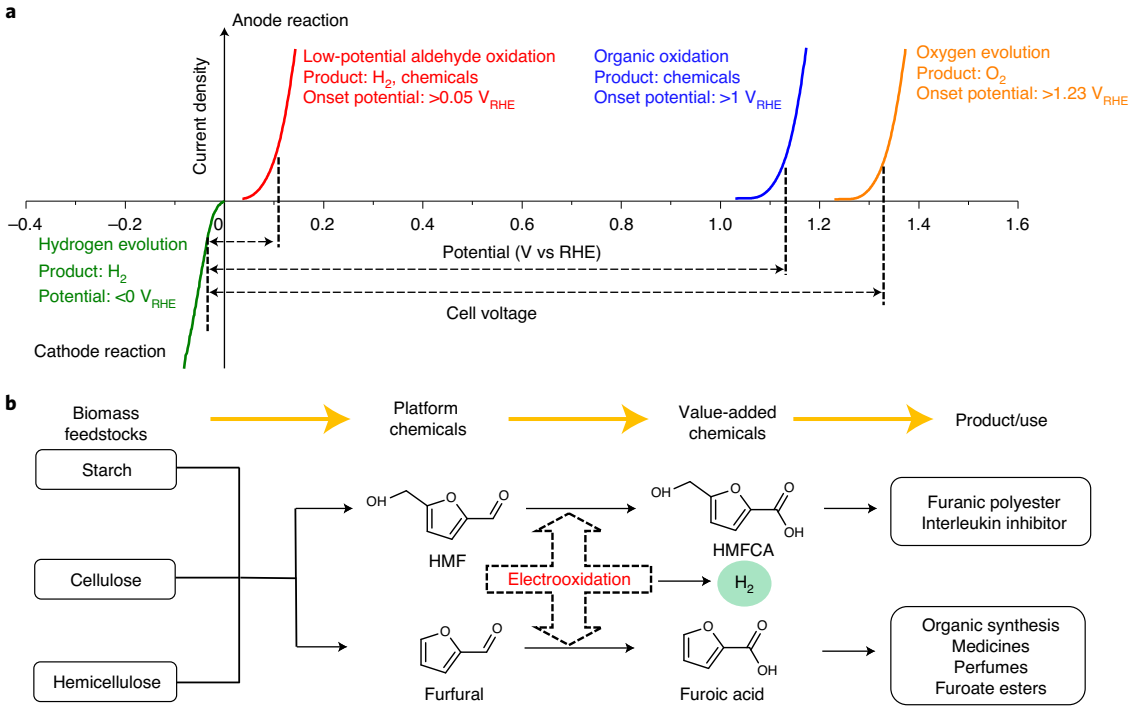

Fig. 1 | Water electrolysis systems with various anode reactions. a, Comparison of various anode reactions for water electrolysis. **b**, Electrochemistry-involved conversion path from biomass feedstock into value-added chemicals.

electrocatalysts to form active (oxy)hydroxide phases. Conceivably, it would be more appealing if the hydrogen atom of the aldehyde group were released as the target H_2 product instead of H_2O, a non-valuable product from the perspective of the atom economy principle in green chemistry. The key to realizing the above-mentioned scenario lies in breaking the C–H bond of the aldehyde group at lower potentials where the resultant hydrogen atom could undergo a Tafel recombination ($*H + *H \rightleftharpoons H_2$) rather than a Volmer oxidation. Fortunately, C–H bond cleavage without any bias potential has been well established in formaldehyde dehydrogenation in a concentrated alkaline solution (for example, 4 M NaOH)[33]. Furthermore, the C–H bond cleavage could be catalysed by various metal nanoparticles such as Cu[34], Ag[35], Au[36] and Pd[37]. Two parallel mechanisms have been identified according to the isotopic composition of the produced H_2 (ref. [38]). In the first mechanism, one hydrogen atom originates from the aldehyde group and the other from water. In the second mechanism, the hydrogen atoms originate from two aldehyde molecules. For other aldehydes such as glyoxylate, only the first mechanism is observed. Regardless of the mechanism, the reported C–H bond cleavage under alkaline conditions suggests the feasibility of converting the hydrogen atom of biomass-derived aldehydes to H_2 rather than H_2O at lower potentials.

In this Article we report a bipolar hydrogen production system in which hydrogen is simultaneously generated at both the cathode and the anode at a low cell voltage of ~0.1 V. This system is realized by coupling the low-potential anodic oxidation of biomass-derived aldehydes with the cathodic HER. The anodic reaction involves the electrocatalytic conversion of aldehydes into the corresponding carboxylate and H_2 on a metallic Cu catalyst at a low onset potential of 0.05 V_{RHE} (Fig. 1a and equation (2)):

$$R\text{–}CHO + 2OH^- \rightleftharpoons R\text{–}COO^- + \frac{1}{2}H_2 + H_2O + e^- \qquad (2)$$

Owing to the low bias potential, the hydrogen atom of the aldehyde group is released as H_2 via Tafel recombination, in contrast to being oxidized to H_2O by the Volmer step as in the case of conventional aldehyde electrooxidation. It is worth mentioning that, as depicted in Fig. 1b, the employed aldehydes (HMF and furfural) are abundant and easily accessible biomass-derived platform chemicals[39] that can be sourced from diverse sustainable biomass feedstocks (such as starch, cellulose and hemicellulose[40]), and the oxidation products (corresponding carboxylic acids) are value-added chemicals and important precursors for a range of products, including drug molecules, perfume and sustainable polymers[24,41]. In the as-assembled electrolyser, the bipolar hydrogen production has an onset voltage below 0.1 V. Interestingly, the Faraday efficiency (FE) for hydrogen production is 100% at both the anode and the cathode, resulting in an apparent FE of 200%. As a result of the low cell voltage and high FE, the electricity input per cubic metre of hydrogen produced in the bipolar hydrogen production system is only ~0.35 kWh, about one-fourteenth of the value for conventional water electrolysis (~5 kWh).

Results

Low-potential aldehyde oxidation. The low-potential aldehyde oxidation reaction is key to our bipolar hydrogen production system. HMF was used as a model substrate for low-potential oxidation in this study. A metallic Cu catalyst with a high electrochemically active surface area (Supplementary Fig. 1) was successfully prepared from Cu_2O by electroreduction, as confirmed by transmission electron microscopy (Supplementary Fig. 2) and X-ray diffraction (Supplementary Fig. 3). Figure 2a presents the linear sweep voltammetry (LSV) curves of the Cu catalyst in 1 M KOH, with and without HMF. In the absence of HMF, an anodic peak centred at 0.52 V_{RHE} is observed, which is associated with the electrooxidation of metallic Cu to Cu_2O (ref. [42]), and no anodic current occurs below 0.45 V_{RHE}. By contrast, the addition of 50 mM HMF results in an obvious anodic current that starts from 0.05 V_{RHE} and reaches

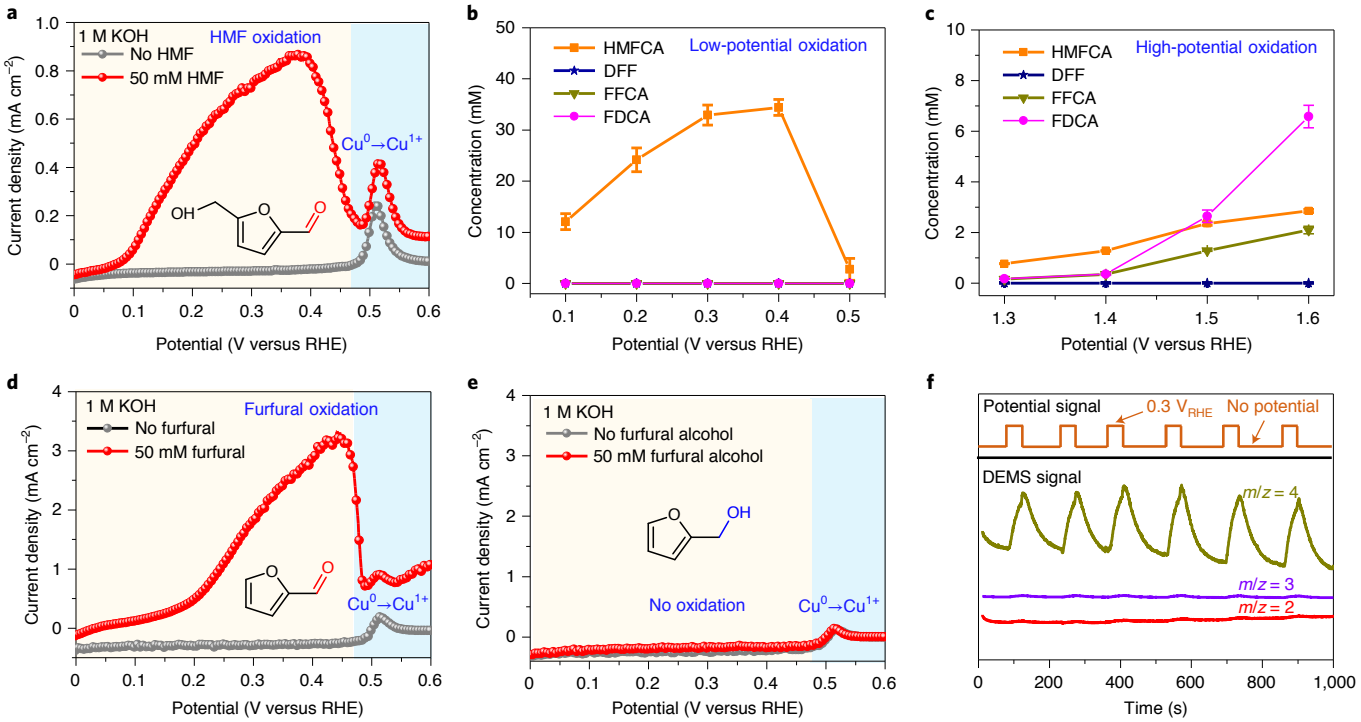

Fig. 2 | Anodic oxidation reaction of biomass-derived aldehydes. a, LSV curves of a Cu-modified glass carbon electrode in 1 M KOH, with (red) and without (grey) 50 mM HMF. **b**,**c**, Product concentration versus applied potential for the low-potential oxidation (**b**) and high-potential oxidation (**c**) of HMF over a Cu foam electrode after electrolysis for 30 min. **d**,**e**, LSV curves of a Cu-modified glass carbon electrode in 1 M KOH with and without 50 mM furfural (**d**) and 50 mM furfural alcohol (**e**). **f**, DEMS signals at $m/z = 2$, 3 and 4 at a pulsed potential of 0.3 V_{RHE} over the Cu catalyst in 1 M KOH with 50 mM deuterated benzaldehyde. Error bars represent the s.d. of at least three independent measurements. In all panels, the pale yellow shaded area indicates the potential window for the low-potential aldehyde oxidation, and the pale blue shaded area indicates the electrooxidation of metallic Cu.

a maximum at ~0.4 V_{RHE}. Further increasing the potential leads to a sharp drop in the current density, which can be attributed to the electrochemical oxidation of the metallic Cu catalyst into Cu_2O and thus deactivates the catalysts for HMF oxidation. Ex situ Raman spectroscopy (Supplementary Fig. 4), Auger electron spectroscopy (Supplementary Fig. 5) and controlled experiments (Supplementary Fig. 6) further confirmed that the metallic Cu is the active phase for the aldehyde oxidation at the low potential window.

Liquid product analysis. To track the distribution of liquid products produced by low-potential HMF oxidation, we analysed the anodic electrolyte after potentiostatic electrolysis using high-performance liquid chromatography (HPLC) and quantified the products using calibration curves (Supplementary Fig. 7). As shown in Fig. 2b, 5-hydroxymethyl-2-furancarboxylic acid (HMFCA) is the exclusive product of HMF oxidation at applied potentials of 0.1–0.4 V_{RHE}, whereas other possible oxidative products such as the dialdehyde 2,5-diformylfuran (DFF), 5-formyl-2-furancarboxylic acid (FFCA) and 2,5-furandicarboxylic acid (FDCA) are absent. A maximum concentration of HMFCA (34.4 ± 1.6 mM) was achieved at 0.4 V_{RHE}. It is noted that HMFCA may be directly generated from a non-faradaic process ($R–CHO + OH^- = R–COO^- + H_2$), as reported in previous works[33–37]. To distinguish between non-faradaic and faradaic processes, we conducted control experiments without applied an anodic potential in the absence or presence of the Cu electrode. As shown in Supplementary Fig. 8, when both catalyst and potential are absent, only trace HMFCA is produced. On applying a bias potential of 0.3 V_{RHE}, again the concentration of HMFCA is a trace. Introduction of the Cu catalyst, without bias potential, can raise the concentration to 3.4 mM. However, this value is only one-tenth of the value (32.9 mM) when both the Cu catalyst and bias potential (0.3 V_{RHE}) are introduced, suggesting that the reaction kinetics of the faradaic process is one order of magnitude faster than that of the non-faradaic process. The calculated FE towards HMFCA in the optimum potential range (0.2–0.4 V_{RHE}) is essentially 100% within experimental error (Supplementary Fig. 9). A time-tracking experiment revealed that the concentration of HMFCA increases with the consumption of HMF as the reaction progresses (Supplementary Fig. 10), with total carbon balances close to 100% (Supplementary Fig. 11).

The products of HMF oxidation at low potential (<0.5 V_{RHE}) differ from those at high potential (>1.0 V_{RHE}), where both the hydroxymethyl and aldehyde groups are oxidized into carboxylic groups[28]. HMF oxidation at high potentials up to 1.6 V_{RHE} (Supplementary Fig. 12) produces FDCA as the main oxidative product, with small amounts of HMFCA and FFCA as oxidative intermediates (Fig. 2c). These results demonstrate that the aldehyde group of HMF can be selectively oxidized to a carboxylic group over the Cu catalyst at low potentials, with the hydroxymethyl group remaining intact. Although oxidation of the aldehyde group can occur at a lower potential, conversion of the hydroxymethyl group still requires higher potentials, thus resulting in HMFCA as the only product for low-potential HMF oxidation.

To further verify the selective oxidation of the aldehyde group of HMF over the Cu catalyst, a series of control experiments were conducted. As shown in Fig. 2d,e, a similar anodic current appears with the addition of furfural (bearing the same aldehyde group as HMF), whereas no current is observed when furfural alcohol (bearing the same hydroxymethyl group as HMF) is added. Furthermore, under a constant potential of 0.3 V_{RHE}, there is no discernible change in the chronoamperometric curve after injecting HMFCA, the exclusive HMF oxidative product observed in

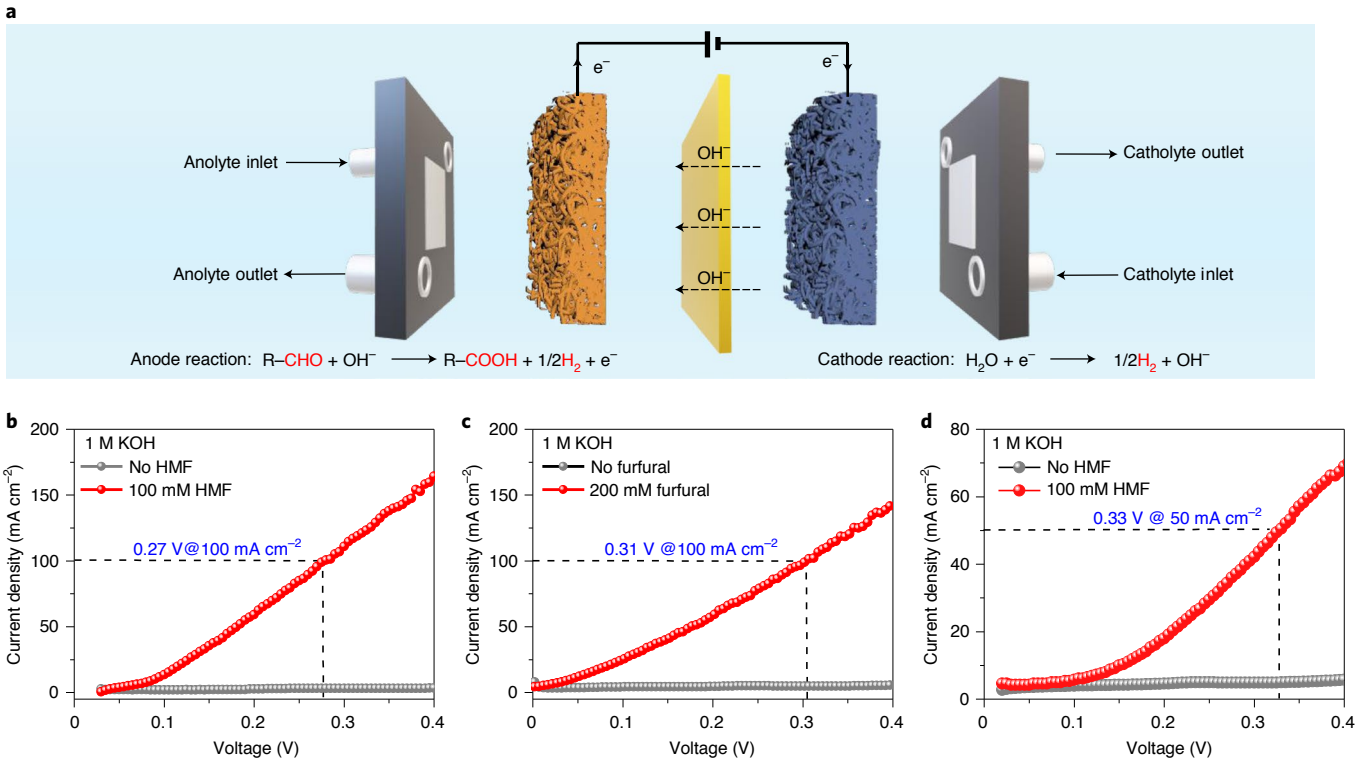

Fig. 3 | The bipolar hydrogen production system. a, Schematic of the two-electrode electrolyser employing low-potential aldehyde oxidation as the anode reaction and HER as the cathode reaction. **b**–**d**, LSV curves of HMF (**b**,**d**) and furfural oxidation (**c**) in the electrolyser using Cu foam as the anode and Pt/C (**b**,**c**) or Ni/Ni foam (**d**) as the cathode.

this work (Supplementary Fig. 13). Corresponding HPLC analysis also confirmed that HMFCA is the sole organic compound in the electrolyte (Supplementary Fig. 14). Taken together, these data substantiate that Cu catalysts can selectively oxidize the aldehyde group of HMF into a carboxylic group at low potentials.

In addition to HMF and furfural, other aromatic aldehydes can also be employed as substrates. As shown in Supplementary Fig. 15, the chronoamperometric curves at $0.3\,V_{RHE}$ steeply increase when 5-formyl-2-furancarboxylic acid, benzaldehyde, 4-hydroxymethyl benzaldehyde and 4-carboxybenzaldehyde are injected, and the corresponding carboxylic acids are detected after electrolysis (Supplementary Fig. 16). Notably, aldehydes with α-H atoms (for example, propionaldehyde) are passive in this reaction (Supplementary Fig. 17). These results demonstrate that Cu-catalysed low-potential aldehyde oxidation can accommodate a diverse range of aromatic aldehydes.

Gaseous product analysis. To identify the gaseous products of the low-potential anodic oxidation reaction, the gas produced at the anode was collected and analysed by gas chromatography. Supplementary Fig. 18 shows that H_2 is exclusively generated concomitant with HMF oxidation over the Cu catalyst, which differs from HMF oxidation at high potentials, where no gas is produced. Differential electrochemical mass spectrometry (DEMS) was conducted to experimentally verify the origin of the H_2 at the anode. Figure 2f shows the DEMS signals for the gaseous products of low-potential aldehyde oxidation using deuterated benzaldehyde (C_6H_5–CDO) as the oxidative substrate. The signal of $m/z=4$ (D_2) shows a sensitive response to the impulse potential, but this scenario is not observed for the signals of $m/z=3$ (HD) or $m/z=2$ (H_2). Furthermore, the FE of the produced H_2 is close to 100% (Supplementary Fig. 19) according to the proposed reaction chemistry (equation (2)). These observations demonstrate that both hydrogen atoms in the produced H_2 gas originate from the aldehyde groups, unlike the mechanism of the non-faradaic process, in which H_2 is formed by combining one aqueous hydrogen atom with one aldehyde-originating hydrogen atom[38].

Notably, the hydrogen atom of the aldehyde group is released as gaseous H_2 in this work, instead of being further oxidized into H_2O, which is a common scenario in conventional aldehyde electrooxidation. To clarify this point from a fundamental viewpoint, we proposed four possible reaction pathways (Supplementary Fig. 20) and performed density functional theory (DFT) calculations on a Cu(111) surface (Supplementary Figs. 21 and 22; the atomic coordinates of the optimized models are provided in Supplementary Data 1). The DFT results show that the reaction pathway via a *gem*-diolate anion intermediate with one proton removed is the most favourable due to the lowest energy barrier of electron-transfer-coupled C–H splitting. Specifically, the resultant hydrogen atoms are preferentially combined to H_2 via the Tafel step ($^*H + {}^*H \rightleftharpoons H_2$) rather than oxidized to H_2O via an alkaline Volmer step ($^*H + OH^- \rightleftharpoons H_2O + e^-$) at the low potential threshold because of the lower energy barrier of the former process on the Cu(111) surface (Supplementary Fig. 21b, inset). These results are in agreement with the scaling relation for the hydrogen oxidation reaction (HOR), with the HOR activity exhibiting a volcano plot versus the hydrogen chemisorption energy (ΔE_H) on the metal surface. As shown in Supplementary Fig. 23a, ΔE_H on the Cu surface is only approximately −0.04 eV, which is almost one order of magnitude lower than that of Pt ($\Delta E_H \approx -0.34$ eV). Given that the HOR activity of Pt-based catalysts with moderate ΔE_H has been well documented, it is hypothesized that the high energy barrier of Volmer oxidation on the Cu(111) surface could be ascribed to the low ΔE_H, thus resulting in Tafel recombination

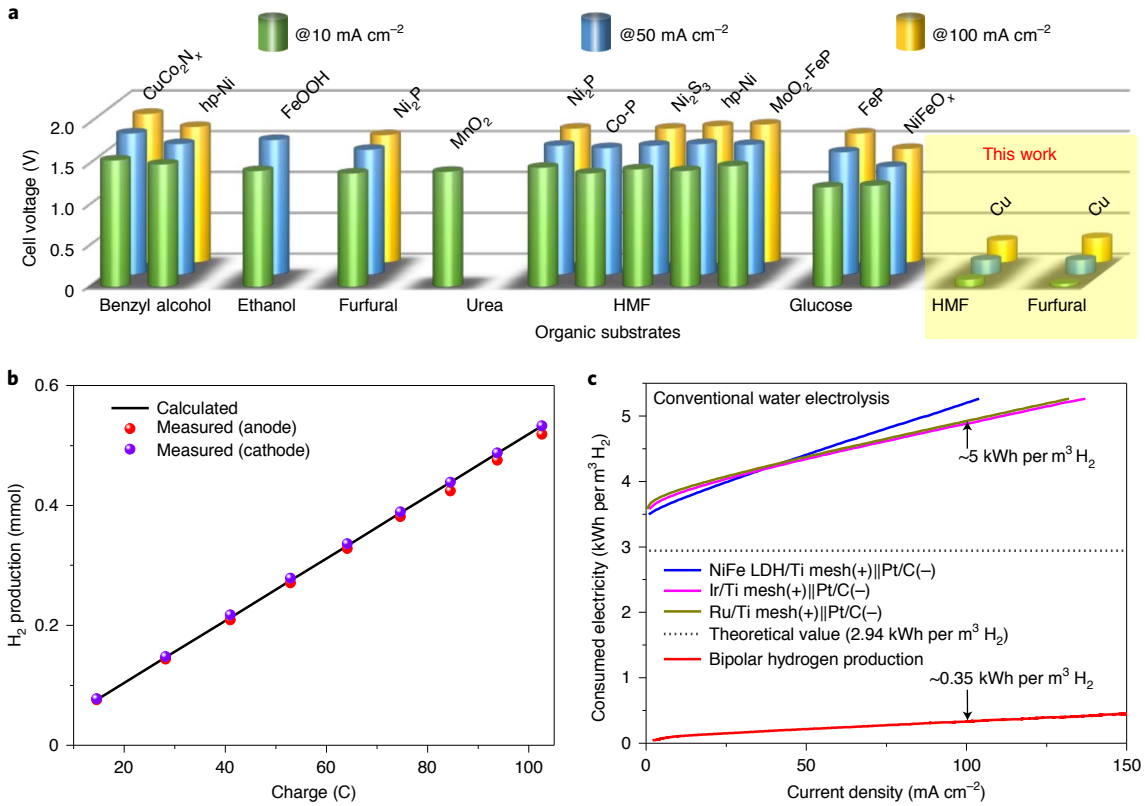

Fig. 4 | Energy efficiency analysis of the bipolar hydrogen production system. a, Comparison of recent electrolysis performances of organic oxidation-coupled hydrogen production in a two-electrode electrolyser. The materials indicated above the bars are the electrocatalysts used for the corresponding organic oxidation reaction. **b**, Comparison of experimentally collected H_2 quantities with those calculated theoretically at the anode and cathode for the bipolar hydrogen production system. The theoretical amount was calculated on the basis of transferred charge assuming a FE of 100% according to equation (5). **c**, Electricity consumed for hydrogen production using conventional water electrolysis and the bipolar hydrogen production system.

being preferential. To support this hypothesis, a control experiment using Ag as the electrode was performed. Because Ag possesses a positive value of ΔE_H ($\Delta E_H = 0.27$ eV), we predict that Tafel recombination of the adsorbed hydrogen atom on the Ag electrode will be similarly more favourable than Volmer oxidation. As shown in Supplementary Fig. 23b, the onset potential of the Ag/carbon cloth electrode for the low-potential aldehyde oxidation is ~0.25 V_{RHE}. Meanwhile, H_2 gas is continuously generated at the surface of the anodic electrode at a constant potential of 0.6 V_{RHE}, as observed in Supplementary Video 1. These results further verify the hypothesis that the low ΔE_H is key to anodic hydrogen production from the Cu electrode.

Taking all the above results into account, it is clear that there are distinct differences between low-potential aldehyde oxidation and conventional aldehyde electrooxidation. The first difference involves the required bias potential. The low-potential aldehyde oxidation can be conducted at a very low potential threshold, with an onset potential of ~0.05 V_{RHE}, whereas conventional aldehyde electrooxidation requires higher potentials, usually >1.0 V_{RHE}. The second difference involves the oxidative products. Owing to the low bias potential, low-potential aldehyde oxidation renders the partial oxidation of the aldehyde group and releases the hydrogen atom into gaseous H_2, with one electron transferred per aldehyde molecule converted. In sharp contrast, conventional aldehyde electrooxidation operated at high potentials leads to complete oxidation of the aldehyde, and the hydrogen atom is further oxidized into useless H_2O, accompanied by two electrons transferred per aldehyde molecule converted. From both economic and sustainability perspectives, we believe that the low-potential aldehyde oxidation is more appealing as an alternative anodic oxidation to replace OER for electrocatalytic hydrogen production.

Electrolyser performance. Coupling this low-potential aldehyde oxidation reaction with a cathodic HER enables a bipolar hydrogen production system, with H_2 production at both the cathode and anode, which is fundamentally different from the conventional system, in which H_2 production takes place only at the cathode (Fig. 3a). The two-electrode electrolyser for bipolar hydrogen production was assembled using Cu foam as the anode and Pt/C as the cathode, with serpentine flow channels, which are beneficial for mass diffusion of the organic substrates. We focused on two biomass-derived aldehydes—HMF and furfural—because they are abundant and easily accessible from sustainable biomass feedstocks (Fig. 1b) and their corresponding carboxylic acid products (HMFCA and 2-furoic acid) are more valuable chemicals. HMFCA is a highly relevant compound for the production of furanic polyesters and the synthesis of interleukin inhibitor[41], and 2-furoic acid is an excellent feedstock in organic synthesis, an important intermediate for medicines and perfumes, and a starting material for furoate esters[24]. Figure 3b presents the electrolyser polarization curves for HMF oxidation. Remarkably, the onset voltage for bipolar hydrogen production is below 0.1 V and a current density of 100 mA cm^{-2} is achieved at a cell voltage of only 0.27 V. When using furfural instead of HMF, a cell voltage of 0.31 V is required to deliver the same current density (Fig. 3c). Furthermore, employing Ni/Ni foam as the cathode (Fig. 3d), a non-noble-metal electrolyser can be assembled and a current density of 50 mA cm^{-2} achieved at a cell voltage of 0.33 V. Remarkably, the cell voltage may be further reduced

if optimized cathodic HER catalysts are employed (for example, single-nickel-atom-modified Pt nanowires[43]).

To investigate the stability of our process, a chronoamperometric experiment lasting for 8 h was performed, showing that the current density suffered a rapid decrease (Supplementary Fig. 24). By checking the electrochemical surface area (ECSA) of the fresh and deactivated Cu electrode (Supplementary Fig. 25), it was found that the deactivation is associated with a decrease in the ECSA, as the degree of decrease in the current density (~60%) is approximately that in the ECSA (~55%). Furthermore, inspection of the morphological evolution by scanning electron microscopy (Supplementary Fig. 26) showed that parts of the bended nanotubes (fresh Cu electrode) aggregated into a large microsphere (deactivated Cu electrode) during the electrochemical process. Despite the low activity, the deactivated Cu electrode still exhibited high selectivity towards H_2 production (Supplementary Fig. 27). In addition, the electrocatalytic activity of the deactivated Cu electrode could be substantially restored by simple cyclic voltammetry activation (Supplementary Fig. 28), with the redox cycle between Cu^0 and Cu^{1+} able to increase the surface roughness and thereby the ECSA (Supplementary Fig. 29). Once the issue of the decreasing surface area is addressed (for example, by electrocatalyst engineering), we believe that our bipolar hydrogen production system will be a promising option for industrial-scale application.

Energy efficiency analysis. From the perspective of energy efficiency, we compared the performances of our systems with those of conventional electrolysers (cathodic hydrogen production) based on different organic substrates (Fig. 4a and Supplementary Table 1). Notably, the voltage required to achieve a target current density in our set-up is much lower than reported for conventional systems. For example, to achieve a current density of 100 mA cm^{-2}, our bipolar hydrogen production system only requires a voltage of 0.27 V, far lower than the values for conventional HMF electrooxidation-coupled hydrogen production systems (for example, 1.6–1.7 V). The FE of the electrolyser for H_2 production was calculated based on the theoretical and experimental amounts of produced H_2 (Supplementary Video 2). The anodic FE was calculated according to equation (1) and the cathodic FE according to $2H_2O + 2e^- \rightarrow 2OH^- + H_2$. As observed in Fig. 4b, the amounts of H_2 produced at the anode and the cathode are close to the theoretical values. As a result, the FE for hydrogen production is doubled, with 100% anodic FE and 100% cathodic FE, thus giving an apparent FE of 200% (two hydrogen atoms, equivalently one hydrogen molecule, are produced for every electron flowing through the electrolyser). In this way, the bipolar system produces twice as much hydrogen as conventional water electrolysis at the same current density. To evaluate the energy conversion efficiency of our bipolar hydrogen production system, conventional water electrolysis was performed for comparison (Supplementary Fig. 30). Conventional water electrolysis requires an electricity input of >3.5 kWh per m^3 of H_2, and the consumption of electricity significantly increases at higher operating current densities (Fig. 4c). In some cases, a higher hydrogen production rate is needed and requires a larger operating current density, which will ultimately increase the electricity consumption and thereby decrease the efficiency of hydrogen production per unit. Thus, it is practical to increase the yield of hydrogen gas at the same current density. In this study, because of its low voltage requirement and doubled hydrogen production rate, our bipolar hydrogen production system only requires an electricity input of ~0.35 kWh per m^3 of H_2 at a current density of 100 mA cm^{-2} using fresh active electrodes, about one-fourteen of the typical value of ~5 kWh per m^3 of H_2 required for conventional water electrolysers[44]. Moreover, based on the data in Fig. 4a (~1.5 V @100 mA cm^{-2} for HMF oxidation), it is estimated that the conventional organic electrolytic system requires an electricity input of ~3.9 kWh per m^3 of H_2, which is also much higher than that of our bipolar hydrogen production system. These results suggest that our bipolar hydrogen production system may be a transformative technology due to its superior energy conversion efficiency.

Conclusions

We have reported a bipolar hydrogen production system that enables hydrogen production from both the anodic low-potential aldehyde oxidation and the cathodic HER. Unlike the conventional high-potential aldehyde oxidation, in which the hydrogen atom of the aldehyde group is oxidized into H_2O, the low-potential aldehyde oxidation is able to release the hydrogen atom as H_2. The bipolar hydrogen production system can start at a low voltage of ~0.1 V and the FEs towards hydrogen production from the anode and cathode are both ~100%. Consequently, this system only requires one-fourteenth of the electricity input of conventional water electrolysers. The developed system provides a promising avenue for the safe, efficient and scalable production of high-purity hydrogen. Although the low-potential aldehyde oxidation reaction can be coupled with many other half reactions, we expect it to find exciting opportunities beyond this field.

Methods

Materials and chemicals. Commercial Cu foam and carbon cloth were purchased from Tianjin EVS Chemical Technology. Potassium hydroxide (analytical reagent, AR), sodium hydroxide (AR), ammonium persulfate (AR), silver nitrate (AR) and hydrochloric acid (AR) were purchased from Sinopharm Chemical Reagent. 5-Hydroxymethyl furfural (98%), furfural (98%), 5-hydroxymethyl-2-furancarboxylic acid (98%), dialdehyde 2,5-diformylfuran (98%), 5-formyl-2-furancarboxylic acid (98%), 2,5-furandicarboxylic acid (98%), 5-formyl-2-furancarboxylic acid (98%), 4-hydroxymethyl benzaldehyde (98%), 4-carboxybenzaldehyde (98%), benzaldehyde (98+%) and deuterated benzaldehyde (98%) were purchased from Sigma-Aldrich. The deionized water was produced by EDI touch-Q/S (HHitech).

Synthesis of the Cu catalysts. The Cu foam was pretreated by wet chemical oxidation and calcinated in Ar gas, followed by electrochemical reduction. In detail, a piece of Cu foam was washed in 2 M HCl solution, ethanol and water, respectively. Afterwards, the Cu foam was immersed in an aqueous solution containing 2.67 M NaOH and 0.13 M $(NH_4)_2S_2O_8$ for 30 min at room temperature to grow $Cu(OH)_2$ nanorods on the surface. The resulting $Cu(OH)_2$/Cu foam was washed in water and dried at 60 °C, then further calcinated at 550 °C for 3 h at a heating rate of 1 °C min^{-1} in Ar gas to obtain Cu_2O/Cu foam. The Cu_2O powder was scraped from the pretreated Cu foam.

Synthesis of the Ag/carbon cloth electrode. Before use, the carbon cloth electrode was calcinated in air at 300 °C for 2 h to increase the surface hydrophilicity. The Ag/carbon cloth electrode was prepared by the wetness method followed by thermal reduction. In detail, a certain amount of $AgNO_3$ aqueous solution (20 mg ml^{-1}) was dropped onto the pretreated carbon cloth, then the cloth was dried at room temperature. The Ag/carbon cloth electrode was obtained by further reduction in H_2/Ar (10 vol% H_2) at 200 °C for 2 h.

Electrochemical measurements. The anode oxidation reaction for the aldehydes was conducted in an electrochemical workstation (Ivium) with a three-electrode configuration in an H-type electrochemical cell, separated using an alkaline polymer electrolyte membrane (Alkymer, w-25). As-synthesized Cu_2O/Cu foam or Cu_2O powder was used as the working electrode, a saturated calomel electrode (SCE) as the reference electrode and a graphite rod as the counter-electrode. The anode electrolyte was 1 M KOH (30 ml), with or without 50 mM substrates, and the cathode electrolyte was 1 M KOH (30 ml). All potentials reported in this work are quoted with respect to the reversible hydrogen electrode (RHE) through RHE calibration, except for the two-electrode electrolyser. Conversion from the SCE reference electrode to RHE was done according to E(versus RHE) = E(versus SCE) + 0.0591 × pH + 0.244. A Cu_2O-powder-modified glass carbon electrode was used as the working electrode for LSV measurements, and Cu_2O/Cu foam was used for the constant electrolysis test. To prepare the Cu_2O-powder-modified glass carbon electrode, 4 mg of powder was added into 750 µl of ethanol, 200 µl of deionized water and 50 µl of Nafion solution (5 wt%), followed by sonication for 30 min, then 10 µl of catalyst suspension was dropped onto the surface of a pre-polished glassy carbon electrode (5 mm in diameter). After being fully dried at room temperature, the catalyst-cast glassy carbon electrode was used as the working electrode for electrochemical measurements. The catalyst loading amount was ~0.2 mg cm^{-2}. Before the electrochemical test, the Cu_2O powder or Cu_2O/Cu foam was treated by electroreduction at −0.4 V for 400 s to obtained active metallic Cu. The LSV curve was recorded at a scan rate of 1 mV s^{-1} and a stirring speed of

1,200 r.p.m. Electrochemical impedance spectroscopy (EIS) tests were measured over a frequency range from 10^5 to 10^{-2} Hz with an a.c. amplitude of 10 mV. The two-electrode electrolysis was performed at room temperature on a single cell with serpentine flow channels (4 cm^2; Sunlaite). The flow rates of the cathode and anode electrolytes were set as 100 and 30 ml min^{-1}, respectively. A scan rate of 5 mV s^{-1} was used for the LSV test and a cell voltage of 0.3 V was applied for the chronoamperometry test. For conventional water electrolysis, the same flow cell was used, except the Cu electrode was replaced by conventional materials for the OER and the anodic organic-containing electrolytes were replaced by 1 M KOH.

Product analysis. The concentrations of organics in the electrolytes were analysed by HPLC with a UV–vis detector, under an applied detection wavelength of 265 nm for all substrates, except furfural. When the products of furfural oxidation were analysed, a wavelength of 220 nm was used. The mobile phase consisted of methanol and 5 mM ammonium formate aqueous solution with a volume ratio of 3:7, and the flow rate was 0.6 ml min^{-1}. A 4.6 mm × 150 mm Shim-pack GWS 5-μm C18 column was used. Each separation lasted for 10 min. The quantification of HMF and its oxidation product was calculated based on the calibration curves of standard compounds with known concentrations. Conversion of the organic substrates and FE were calculated on the basis of the following equations:

$$\text{Conversion}\,(\%) = \left(1 - n\,[\text{mole}]_{\text{after electrolysis}}/n\,[\text{mole}]_{\text{before electrolysis}}\right) \times 100 \quad (3)$$

$$\text{Faraday efficiency}\,(\%) = \left(n\,[\text{mole}]_{\text{experimentally produced}}/n\,[\text{mole}]_{\text{theoretically produced}}\right) \times 100 \quad (4)$$

where n[mole] is the mole number of the substrate. The theoretically produced amount was calculated on the basis of

$$n\,[\text{mole}]_{\text{theoretically produced}} = Q/(n \times F) \quad (5)$$

where Q is the transferred charge, n is the number of electrons transferred for each product molecule and F is Faraday's constant (96,485 C mol^{-1}).

For qualitative analysis of the gaseous product, the gas was collected into a gasbag (1 l) by purging with nitrogen through the anode of the H-type electrochemical cell. The collected gas was analysed by gas chromatography, with a thermal conductivity detector and a TDX-01 column. The temperature of the gasifier, the oven and the detector was set to 120 °C. Argon was used as the carrier gas for gas chromatography and the flow rate was 30 ml min^{-1}. The gas product was further checked in the electrolytic cell of an in situ DEMS set-up (Shanghai Linglu Instrument Equipment). A Teflon film separated the electrolyte from the vacuum system to minimize the amount of aqueous solvents entering the mass spectrometer. The vacuum system consisted of two dry pumps and one turbo pump, and the vacuum was maintained below 2×10^{-4} Pa. Trace products in the reaction process could be detected by in situ DEMS. The preparation process for the working electrode was the same as for the Cu-modified glass carbon electrode. The quantity of hydrogen produced in the flow cell was determined by a water displacement method. Specifically, a three-necked flask was used as the vessel of the electrolyte. One of the three necks was connected to the electrolyte inlet of the flow cell by a peristaltic pump, and another neck was connected to the electrolyte outlet. The third neck was connected to a graduated cylinder, which was filled with water and submerged inversely in a water-filled beaker (500 ml). Once hydrogen was produced in the flow cell, the pressure in the three-necked flask rose and forced the gas into the inverted graduated cylinder to replace the water. The volume of water discharged was approximately equal to the volume of produced hydrogen.

The electricity consumption per m^3 of H_2 produced (W, kWh per m^3 H_2) was calculated as

$$W = (n \times F \times U \times 1,000)/(3,600 \times V_m) \quad (6)$$

where n is the number of electrons transferred for each product molecule, U is the applied voltage and V_m is the molar volume of gas at normal temperature and pressure (22.4 mol l^{-1}). It is noted that $n = 1$ in our bipolar hydrogen production system and $n = 2$ for conventional water electrolysis and conventional organic electrooxidation-coupled hydrogen production systems.

Characterization. The morphology and microstructure of the catalysts were observed by transmission electron microscopy (FEI, F20 S-TWIX). The crystal phase of the materials was examined by X-ray diffraction (Bruker, D8-Advance X-ray diffractometer, Cu Kα, $\lambda = 1.5406$ Å). Auger electron spectroscopy analysis was performed on an ESCALAB 250Xi X-ray photoelectron spectrometer using Mg as the excitation source. Raman spectroscopy was carried on a WiTec probe microscope using 532 nm radiation.

Computation methods. All DFT computations were performed using the Vienna ab initio simulation package (VASP)[45]. The ion–electron interaction was described with the projector-augmented plane-wave (PAW) method[46,47]. The exchange-correlation energy was expressed using the Perdew–Burke–Ernzerhof (PBE) functional with the generalized gradient approximation (GGA)[48]. We set the cutoff energy to 460 eV and sampled the Brillouin zone at 3 × 3 × 1 for geometry optimization. To avoid interlayer interaction, the vacuum thickness was set to 20 Å. The systems were relaxed until the energy and force reached the convergence threshold at 10^{-5} eV and 0.01 eV $Å^{-1}$, respectively. We calculated the Gibbs free energy for the alkaline HMF oxidation process according to the computational hydrogen electrode model[49]. Solvation effects were also considered with the Poisson–Boltzmann implicit solvation model, and the dielectric constant of water was taken to be 80 (ref. [50]). The van der Waals interactions were included utilizing the DFT-D3 method[51]. The climbing-image nudged elastic band (CI-NEB) method was used to obtain the energy barrier for the alkaline HMF oxidation reaction on the Cu(111) surface[52].

The pH effect on the reaction energy and activation energy was also evaluated in this work. In a proton–electron transfer reaction process with water as the proton source, the pH changes the chemical potential of OH^- through its configurational entropy, while the absolute potential versus the standard hydrogen electrode (that is, U_{SHE}) affects the chemical potential of the electron, e^-. For the kinetic energy barrier, the transition state is assumed to have no entropic contributions and its value only depends on the potential via a pH-independent transfer coefficient α, so the energy barrier can be expressed as

$$\begin{aligned} G^{HMF} &= \mu_{XH^*} + \mu_{OH} - \mu_{H_2O} + \mu_{e^-,U} + \mu_{X^*} \\ &= \mu_{XH^*} + \left(\mu^0_{OH} - 2.3k_BT(14 - \text{pH})\right) \\ &\quad -\left(\mu_{H_2O} + \left(\mu_{e^-,U} - eU_{SHE}\right) + \mu_{X^*}\right) \\ &= \Delta G^{HMF}_0 + eU_{SHE} + 2.3k_BT\text{pH} \\ &= \Delta G^{HMF}_0 + eU_{SHE} \end{aligned} \quad (7)$$

$$\begin{aligned} G^{HMF}_a &= \mu_{TS} + \mu_{\alpha e^-,U} - \left(\mu_{HMF} + \mu_{e^-,U} + \mu_{X^*}\right) \\ &= \mu_{TS} + \left(\mu_{\alpha e^-,U} - \alpha eU_{SHE}\right) - \left(\mu_{HMF} + \left(\mu_{e^-,U} - eU_{SHE}\right) + \mu_{X^*}\right) \\ &= G^{HMF}_a + \beta eU_{SHE} \\ &= G^{HMF}_{a,0} + \beta eU_{RHE} - \beta 2.3k_BT\text{pH} \end{aligned} \quad (8)$$

where μ_{X^*} is the chemical potential of species X*, G^{HMF}_a and G^{HMF} are the activation energy and reaction energy at 0 V, α is the charge in the transition state that gives the potential dependence ($\beta = 1 - \alpha$), T is temperature and k_B is the Boltzmann constant. The reaction energies are thus affected by the pH shifts, while the energy barriers decrease with increasing pH (ref. [53]).

Data availability

The data that support the findings of this study are included in the published article and its Supplementary Information. All other data are available from the authors upon reasonable request. Source data are provided with this paper.

Received: 5 April 2021; Accepted: 10 November 2021;
Published online: 22 December 2021

References

1. Chu, S. & Majumdar, A. Opportunities and challenges for a sustainable energy future. *Nature* **488**, 294–303 (2012).
2. Lin, L. et al. Low-temperature hydrogen production from water and methanol using Pt/α-MoC catalysts. *Nature* **544**, 80–83 (2017).
3. Tian, X. L. et al. Engineering bunched Pt-Ni alloy nanocages for efficient oxygen reduction in practical fuel cells. *Science* **366**, 850–856 (2019).
4. Gong, K. P., Du, F., Xia, Z. H., Durstock, M. & Dai, L. M. Nitrogen-doped carbon nanotube arrays with high electrocatalytic activity for oxygen reduction. *Science* **323**, 760–764 (2009).
5. Nikolaidis, P. & Poullikkas, A. A comparative overview of hydrogen production processes. *Renew. Sustain. Energy Rev.* **67**, 597–611 (2017).
6. Lin, F. et al. Electrocatalytic hydrogen evolution of ultrathin Co-Mo_5N_6 heterojunction with interfacial electron redistribution. *Adv. Energy Mater.* **10**, 2002176 (2020).

7. Wu, L. et al. Heterogeneous bimetallic phosphide Ni_2P-Fe_2P as an efficient bifunctional catalyst for water/seawater splitting. *Adv. Funct. Mater.* **31**, 2006484 (2020).
8. Mahmood, J. et al. An efficient and pH-universal ruthenium-based catalyst for the hydrogen evolution reaction. *Nat. Nanotechnol.* **12**, 441–446 (2017).
9. Li, H. et al. Activating and optimizing MoS_2 basal planes for hydrogen evolution through the formation of strained sulphur vacancies. *Nat. Mater.* **15**, 48–53 (2016).
10. Zhang, B. et al. High-valence metals improve oxygen evolution reaction performance by modulating 3*d* metal oxidation cycle energetics. *Nat. Catal.* **3**, 985–992 (2020).
11. Kuai, C. et al. Phase segregation reversibility in mixed-metal hydroxide water oxidation catalysts. *Nat. Catal.* **3**, 743–753 (2020).
12. Oener, S. Z., Foster, M. J. & Boettcher, S. W. Accelerating water dissociation in bipolar membranes and for electrocatalysis. *Science* **369**, 1099–1103 (2020).
13. Rausch, B., Symes, M. D., Chisholm, G. & Cronin, L. Decoupled catalytic hydrogen evolution from a molecular metal oxide redox mediator in water splitting. *Science* **345**, 1326–1330 (2014).
14. You, B., Han, G. Q. & Sun, Y. J. Electrocatalytic and photocatalytic hydrogen evolution integrated with organic oxidation. *Chem. Commun.* **54**, 5943–5955 (2018).
15. Chen, L., Dong, X. L., Wang, Y. G. & Xia, Y. Y. Separating hydrogen and oxygen evolution in alkaline water electrolysis using nickel hydroxide. *Nat. Commun.* **7**, 11741 (2016).
16. Chen, G. F., Luo, Y. R., Ding, L. X. & Wang, H. H. Low-voltage electrolytic hydrogen production derived from efficient water and ethanol oxidation on fluorine-modified FeOOH anode. *ACS Catal.* **8**, 526–530 (2018).
17. Chen, Y. X. et al. Nanotechnology makes biomass electrolysis more energy efficient than water electrolysis. *Nat. Commun.* **5**, 4036 (2014).
18. You, B., Liu, X., Liu, X. & Sun, Y. Efficient H_2 evolution coupled with oxidative refining of alcohols via a hierarchically porous nickel bifunctional electrocatalyst. *ACS Catal.* **7**, 4564–4570 (2017).
19. Zheng, J. et al. Hierarchical porous NC@CuCo nitride nanosheet networks: highly efficient bifunctional electrocatalyst for overall water splitting and selective electrooxidation of benzyl alcohol. *Adv. Funct. Mater.* **27**, 1704169 (2017).
20. Huang, H. et al. Ni, Co hydroxide triggers electrocatalytic production of high-purity benzoic acid over 400 mA cm^{-2}. *Energy Environ. Sci.* **13**, 4990–4999 (2020).
21. Chen, S., Duan, J. J., Vasileff, A. & Qiao, S. Z. Size fractionation of two-dimensional sub-nanometer thin manganese dioxide crystals towards superior urea electrocatalytic conversion. *Angew. Chem. Int. Ed.* **55**, 3804–3808 (2016).
22. Liu, W. J. et al. Efficient electrochemical production of glucaric acid and H_2 via glucose electrolysis. *Nat. Commun.* **11**, 265 (2020).
23. Du, P. Y., Zhang, J. J., Liu, Y. H. & Huang, M. H. Hydrogen generation from catalytic glucose oxidation by Fe-based electrocatalysts. *Electrochem. Commun.* **83**, 11–15 (2017).
24. Jiang, N. et al. Electrocatalysis of furfural oxidation coupled with H_2 evolution via nickel-based electrocatalysts in water. *ChemNanoMat* **3**, 491–495 (2017).
25. Jiang, N., You, B., Boonstra, R., Rodriguez, I. M. T. & Sun, Y. J. Integrating electrocatalytic 5-hydroxymethylfurfural oxidation and hydrogen production via Co-P-derived electrocatalysts. *ACS Energy Lett.* **1**, 386–390 (2016).
26. You, B., Jiang, N., Liu, X. & Sun, Y. J. Simultaneous H_2 generation and biomass upgrading in water by an efficient noble-metal-free bifunctional electrocatalyst. *Angew. Chem. Int. Ed.* **55**, 9913–9917 (2016).
27. You, B., Liu, X., Jiang, N. & Sun, Y. J. A general strategy for decoupled hydrogen production from water splitting by integrating oxidative biomass valorization. *J. Am. Chem. Soc.* **138**, 13639–13646 (2016).
28. Zhang, N. N. et al. Electrochemical oxidation of 5-hydroxymethylfurfural on nickel nitride/carbon nanosheets: reaction pathway determined by in situ sum frequency generation vibrational spectroscopy. *Angew. Chem. Int. Ed.* **58**, 15895–15903 (2019).
29. Zhou, B. et al. Platinum modulates redox properties and 5-hydroxymethylfurfural adsorption kinetics of $Ni(OH)_2$ for biomass upgrading. *Angew. Chem. Int. Ed.* **60**, 22908–22914 (2021).
30. Lu, Y. et al. Identifying the geometric site dependence of spinel oxides for the electrooxidation of 5-hydroxymethylfurfural. *Angew. Chem. Int. Ed.* **59**, 19215–19221 (2020).
31. Lu, Y. et al. Tuning the selective adsorption site of biomass on Co_3O_4 by Ir single atoms for electrosynthesis. *Adv. Mater.* **33**, 2007056 (2021).
32. Nam, D.-H., Taitt, B. J. & Choi, K.-S. Copper-based catalytic anodes to produce 2,5-furandicarboxylic acid, a biomass-derived alternative to terephthalic acid. *ACS Catal.* **8**, 1197–1206 (2018).
33. Kapoor, S., Barnabas, F. A., Sauer, M. C., Meisel, D. & Jonah, C. D. Kinetics of hydrogen formation from formaldehyde in basic aqueous solutions. *J. Phys. Chem.* **99**, 6857–6863 (1995).
34. Bi, Y. & Lu, G. Nano-Cu catalyze hydrogen production from formaldehyde solution at room temperature. *Int. J. Hydrogen Energy* **33**, 2225–2232 (2008).
35. Gao, S. et al. Immobilizing AgPd alloy on Vulcan XC-72 carbon: a novel catalyst for highly efficient hydrogen generation from formaldehyde aqueous solution. *RSC Adv.* **6**, 105638–105643 (2016).
36. Pan, X. et al. A novel biomass assisted synthesis of Au-$SrTiO_3$ as a catalyst for direct hydrogen generation from formaldehyde aqueous solution at low temperature. *Int. J. Hydrogen Energy* **40**, 1752–1759 (2015).
37. Hu, H., Jiao, Z., Ye, J., Lu, G. & Bi, Y. Highly efficient hydrogen production from alkaline aldehyde solutions facilitated by palladium nanotubes. *Nano Energy* **8**, 103–109 (2014).
38. Kapoor, S. & Naumov, S. On the origin of hydrogen in the formaldehyde reaction in alkaline solution. *Chem. Phys. Lett.* **387**, 322–326 (2004).
39. Lucas, F. W. S. et al. Electrochemical routes for the valorization of biomass-derived feedstocks: from chemistry to application. *ACS Energy Lett.* **6**, 1205–1270 (2021).
40. Werpy, T. A., Holladay, J. E. & White, J. F. *Top Value Added Chemicals from Biomass: I. Results of Screening for Potential Candidates from Sugars and Synthesis Gas* Technical Report (US Department of Energy, 2004); https://doi.org/10.2172/15008859
41. Zhao, D. Y., Rodriguez-Padron, D., Luque, R. & Len, C. Insights into the selective oxidation of 5-hydroxymethylfurfural to 5-hydroxymethyl-2-furan carboxylic acid using silver oxide. *ACS Sustain. Chem. Eng.* **8**, 8486–8495 (2020).
42. Deng, Y. L., Handoko, A. D., Du, Y. H., Xi, S. B. & Yeo, B. S. In situ Raman spectroscopy of copper and copper oxide surfaces during electrochemical oxygen evolution reaction: identification of Cu-III oxides as catalytically active species. *ACS Catal.* **6**, 2473–2481 (2016).
43. Li, M. et al. Single-atom tailoring of platinum nanocatalysts for high-performance multifunctional electrocatalysis. *Nat. Catal.* **2**, 495–503 (2019).
44. Ursua, A., Gandia, L. M. & Sanchis, P. Hydrogen production from water electrolysis: current status and future trends. *Proc. IEEE* **100**, 410–426 (2012).
45. Kresse, G. & Hafner, J. Ab initio molecular dynamics for liquid metals. *Phys. Rev. B* **47**, 558–561 (1993).
46. Blochl, P. E. Projector augmented-wave method. *Phys. Rev. B* **50**, 17953–17979 (1994).
47. Kresse, G. & Joubert, D. From ultrasoft pseudopotentials to the projector augmented-wave method. *Phys. Rev. B* **59**, 1758–1775 (1999).
48. Perdew, J., Burke, K. & Ernzerhof, M. Generalized gradient approximation made simple. *Phys. Rev. Lett.* **77**, 3865–3868 (1996).
49. Nørskov, J. K. et al. Origin of the overpotential for oxygen reduction at a fuel-cell cathode. *J. Phys. Chem. B* **108**, 17886–17892 (2004).
50. Mathew, K., Sundararaman, R., Letchworth-Weaver, K., Arias, T. A. & Hennig, R. G. Implicit solvation model for density-functional study of nanocrystal surfaces and reaction pathways. *J. Chem. Phys.* **140**, 084106 (2014).
51. Grimme, S. Semiempirical GGA-type density functional constructed with a long-range dispersion correction. *J. Comput. Chem.* **27**, 1787–1799 (2006).
52. Mills, G. & Jonsson, H. Quantum and thermal effects in H_2 dissociative adsorption: evaluation of free energy barriers in multidimensional quantum systems. *Phys. Rev. Lett.* **72**, 1124–1127 (1994).
53. Liu, X. et al. pH effects on the electrochemical reduction of CO_2 towards C_2 products on stepped copper. *Nat. Commun.* **10**, 32 (2019).

Acknowledgements

This work is supported by the National Key R&D Program of China (grant nos. 2021YFA1500900 (S.W.)), the National Natural Science Foundation of China (grants nos. 21902047 (Y.Z.), 21825201 (S.W.) and U19A2017 (S.W.)) and the Provincial Natural Science Foundation of Hunan (grants nos. 2016TP1009 (S.W.) and 2020JJ5045 (S.W.)).

Author contributions

S.W. and X.-Z.F. conceived the project. T.W. and L.T. carried out most of the experiments and co-wrote the manuscript. X.Z. and Y.L. performed the theoretical calculations. C.C., W.C., S.D. and Y.Z. performed partial characterization of the materials. B.Z., D.W., P.L., C.X., W.L., Y.W., R.C. and Y.Z. participated in data analysis. X.D. provided some important and constructive suggestions to this work. All authors discussed the results and commented on the manuscript.

Competing interests

The authors declare no competing interests.

Additional information

Supplementary information The online version contains supplementary material available at https://doi.org/10.1038/s41929-021-00721-y.

Correspondence and requests for materials should be addressed to Yuqin Zou, Xian-Zhu Fu, Yafei Li, Xiangfeng Duan or Shuangyin Wang.

Peer review information *Nature Catalysis* thanks Carlos Ponce de León, Lin Zhuang and the other, anonymous, reviewer(s) for their contribution to the peer review of this work.

Reprints and permissions information is available at www.nature.com/reprints.

Publisher's note Springer Nature remains neutral with regard to jurisdictional claims in published maps and institutional affiliations.

© The Author(s), under exclusive licence to Springer Nature Limited 2021